Accepted Manuscript

X-ray tomography studies on porosity and particle size distribution in cast in-situ Al-Cu-TiB$_2$ semi-solid forged composites

James Mathew, Animesh Mandal, Jason Warnett, Mark A. Williams, M. Chakraborty, Prakash Srirangam

Please cite this article as: Mathew James, Mandal Animesh, Warnett Jason, Williams Mark A., Chakraborty M, Srirangam Prakash, X-ray tomography studies on porosity and particle size distribution in cast in-situ Al-Cu-TiB$_2$ semi-solid forged composites, *Materials Characterization* (2016), doi: 10.1016/j.matchar.2016.05.010
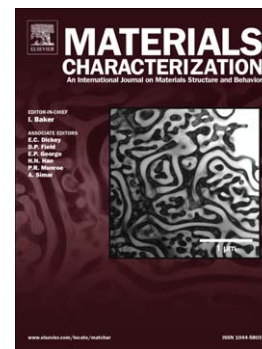
X-ray tomography studies on porosity and particle size distribution in cast in-situ Al-Cu-TiB$_2$ semi-solid forged composites

James Mathew[1], Animesh Mandal[1], Jason Warnett[3], Mark A. Williams[3], M. Chakraborty[2], Prakash Srirangam[3*]

[1] School of Minerals, Metallurgical and Materials Engineering, Indian Institute of Technology, Bhubaneswar, India

[2] Department of Metallurgical and Materials Engineering, Indian Institute of Technology, Kharagpur, India

[3] WMG, University of Warwick, Coventry, CV4 7AL, UK

*Corresponding author: *Prakash Srirangam* (p.srirangam@warwick.ac.uk)

Tel: +044-2476573662

Abstract

X-ray computed tomography (XCT) was used to characterise the internal microstructure and clustering behaviour of TiB$_2$ particles in in-situ processed Al-Cu metal matrix composites prepared by casting method. Forging was used in semi-solid state to reduce the porosity and to uniformly disperse TiB$_2$ particles in the composite. Quantification of porosity and clustering of TiB$_2$ particles was evaluated for different forging reductions (30% and 50% reductions) and compared with an as-cast sample using XCT. Results show that the porosity content was decreased by about 40% due to semi-solid forging as compared to the as-cast condition. Further, XCT results show that the 30% forging reduction resulted in greater uniformity in distribution of TiB$_2$ particles within the composite compared to as-cast and the 50% forge reduction in semi-solid state. These results show that the application of forging in semi-solid state enhances particle distribution and reduces porosity formation in cast in-situ Al-Cu-TiB$_2$ metal matrix composites.

Keywords: X-ray computed tomography, Al-Cu alloy, TiB$_2$ particles, Metal matrix composite.

1. Introduction

The demand for the development of light weight metal matrix composites (MMCs) has been increasing in automotive and aerospace sectors as their implementation results in greater fuel efficiency and hence a reduction in greenhouse gas emissions [1]. Aluminium based MMCs play an important role towards achieving these goals due to their excellent high strength to weight ratio, fracture toughness, electrical and thermal conductivity [2-4]. MMCs are usually prepared by addition of reinforcement particles externally into the metal matrix. This method of adding reinforcement particles externally into the molten metal encounters with problems such as poor wettability, weak interfacial bonding and inhomogeneous distribution of particles which ultimately results in inferior mechanical and performance properties of MMCs [5,6,7]. One alternative is to cast MMCs using in-situ processing methods which help in improving the wettability, uniform dispersion of particles and reduces unwanted reactions between matrix and reinforcements particles [5,6]. Synthesis of aluminium based MMCs with in-situ TiB_2 particles by flux assisted synthesis routes (FAS) using K_2TiF_6 and KBF_4 salts (liquid metallurgy route) has garnered significant interest in this class of materials [8-10]. However, one of the main concerns with Al based TiB_2 in-situ composites is to ensure uniform dispersion of TiB_2 particles as particles have a great tendency to cluster forming agglomerates which ultimately degrades the mechanical and performance properties of composites [2,3,11,12,13]. Previous research studies have shown that semi-solid processing of composites not only decreases porosity, but also greatly helps in uniform dispersion of particles in the alloy matrix. [14–16]. Sidhalingeswara and Herbert et al studied clustering behaviour of particles in Al-4.5Cu-5TiB_2 semi-solid rolled composites and observed that after a critical number of passes, the particles tend to recluster and eventually resulted in formation of agglomerates in MMCs [17,18]. Though semi-solid processing of Al-Cu-TiB_2 is an excellent synthesis method, but still there are few challenges that needs to be taken care such as (i) precise control of liquid fraction at the grain boundaries (ii) microstructure control, (iii) homogenization of matrix composition and most importantly (iv) redistribution of TiB_2 particles [17, 18].

Understanding the porosity formation and dispersion of reinforcement particles/clusters in bulk MMCs is essential to understand the mechanical and performance properties of MMCs. Though 2D image based microscopy techniques such as optical and SEM characterisation provides internal microstructural information of MMCs, it is difficult to obtain quantified information on porosity and particle size distribution using these techniques [19-21]. X-ray computed tomography (XCT) is a non-destructive technique which can provide a three dimensional (3D) visualisation of internal structure of inhomogeneities representative of bulk sample [22–25]. Hamilton et al [11,26] used XCT to study TiB_2 particle clustering and its distribution in Al-TiB_2 composites. Recently, Chen et al [12] used synchrotron XCT to study TiB_2 particles in in-situ Al-TiB_2 composites. In this publication, we present the application of XCT to visualise and quantify the porosity and TiB_2 particle distribution in cast in-situ Al-TiB_2 semi-solid forged composites and compare with an as-cast condition.

2. Experimental details

2.1 Processing of Al-4.5 wt% Cu-5 wt% TiB_2 in-situ composite

The Al-4.5 wt % Cu-5 wt % TiB_2 composite was synthesized using flux assisted synthesis (FAS) technique where halide salts, K_2TiF_6 and KBF_4 are added to molten Al-4.5Cu alloy at 800 °C. The exothermic reaction within the melt results in formation of titanium-diboride (TiB_2) particles. The melt was stirred intermittently every 10 minutes to ensure complete reaction and homogenous distribution of TiB_2 particles. After a reaction time of one hour, lighter dross was decanted and the melt was degassed using C_2Cl_6. The composite melt was finally poured into rectangular mild steel mould and subsequently samples of 10 mm x 10 mm x 60 mm were machined for forging in semi-solid state. Two samples in as-cast condition and four samples from thixo-forged condition were selected for microstructural and XCT characterisation studies.

3

The thixo-forging was carried out using 80 ton hydraulic press, at 150 kg/cm^2 load at a ram speed of 20 mm/sec. The specimens were subjected to forging up to 30% and 50% reduction in the semi-solid range. The semi-solid forging temperature used was 632°C corresponding to a 0.3 volume fraction of liquid (V_{fl}) in the composite. The samples were soaked at 632°C for 10 minutes prior to forging. The K-type thermocouples were used to monitor the temperatures with an accuracy of $\pm$ 2 °C.

2.2 Optical microscopy

Optical microscopy studies were carried out on mechanically polished samples using standard metallographic procedures. The polished samples were anodised with a Barker's reagent (1.8% HBF$_4$ in water) applying 23V dc for up to 1 minute. The dark and bright field microphotographs were captured using a NIKON (Model: ECLIPSE LV150N) metallurgical microscope.

2.3 Scanning electron microscopy (SEM)

SEM studies were carried out to obtain higher magnification images for better visualisation of microstructure of composite samples. . Micrographs were captured by a field emission scanning electron microscope (FESEM) using Zeiss, Carl Zeiss SMT AG instrument coupled with energy dispersive X-ray spectrometer (EDS).

2.4 X ray computed tomography (XCT)

X-ray computed tomography was carried out using the Zeiss versa 520 at WMG, University of Warwick, UK. The samples were prepared as 1 mm diameter cylinders and scanned under the conditions given in Table 1. To achieve high resolution, a 20x lens optic at the detector was used. Since the as-cast sample contains significantly larger features with greater pores and agglomeration of TiB$_2$ particles, a lower resolution was employed moving the detector closer to the sample and binning pixels 2x2, seen to be sufficient in an ortho slice of the scan in figure 3. The advantage of

4

binding pixels during the scanning process is the increased amount of flux received by the detector that leads to shorter scan times. The detector consists of 2000 x 2000 pixels resulting in a 380 μm and 820 μm field of view for the 0.3 V_{fl}, 30% reduction/0.3 V_{fl}, 50% reduction and as-cast samples respectively. The images were reconstructed using the Zeiss reconstruction software that employs a filtered back projection algorithm [35]. The resultant volumes were then segmented and analysed in Avizo 9.0 (FEI, USA; http://www.fei.com/software/avizo3d).

Table 1:

Scanning parameter	As-cast	0.3V_{fl}, 30% / 50% reduction
Voltage (kV)	110	110
Current (μA)	79	79
Exposure (s)	15	32
Filter (Quartz, mm)	1	1
Number of Projections	3201	3201
Pixel binning	X2	X1
Voxel size (nm)	820	190

3. Results and Discussion

Figure 2 shows the optical and SEM microscopy images for semi-solid processed Al-Cu-TiB$_2$ in-situ composites. Figure 2 (a-c) represents optical images at low magnification, while figure 2(d-f) represents SEM images at higher magnifications. As shown in figure 2(a) the as-cast microstructure of Al-4.5Cu-5TiB$_2$ composite shows TiB$_2$ clusters of varying size randomly distributed in the matrix. Deformation of composite up to 30% results in significant fragmentation of the TiB$_2$ particles within the matrix (Figure 2b). Further increase in deformation up to 50% leads to considerable alignment of TiB$_2$ particles in the direction normal to forging direction, though few agglomerates still persist in the microstructure. The redistribution of TiB$_2$ particles could be due to multiple phenomena that occur simultaneously such as - disruption of their grain boundary network by both viscous flow of liquid and either deformation or fragmentation of unmelted solid grains

5

during semi-solid state forging. It is evident from microstructures of the deformed samples that the TiB_2 particles were driven from their original locations at grain boundaries by viscous drag of the intergranular liquid due to compression during forging.

Figure 3 shows the two dimensional XY orthogonal slices obtained from XCT measurements for semi-solid processed Al-Cu-TiB_2 in-situ composites. The as-cast composite (Figure 3a) shows the presence of pores, clusters of TiB_2 particles and elongated Al_3Ti particles. Deformation up to 30% results in a significant reduction in porosity and the alignment of TiB_2 particles in the form of strings as shown in figure 3b. The average size of the pore in as-cast condition was found to be 165.5 μm^2, an order of magnitude greater than the average 14.1 μm^2 in 30% deformed condition. Further increase in deformation up to 50% (Figure 3c) resulted in a higher degree of fragmentation of TiB_2 clusters as shown in figure 3c. Also, there was no evidence of Al_3Ti particles in the semi-solid processed composite which could be due to complete dissolution of Al_3Ti particles in the liquid at forging temperature.

To segment the volumes first a match contrast function was applied to the $V_{fl} = 0.3$, 30% reduction and as-cast volumes with $V_{fl} = 0.3$, 50% reduction as the reference volume. The function applies equalization and normalization to the target volume such that it has an almost homogeneous dynamic range as the reference volume. In doing so the same intensity-based image analysis can be applied to all data sets such that the segmentation is comparable. The implication of applying the function is shown in Figure 4 for the target volume $V_{fl} = 0.3$, 30% reduction. It can be seen that the overall grey level histogram for the volume now has its global maximum at a similar position to the reference volume. The effect on the grey values is more directly shown by observation of line profiles of grey values within the volume. As seen in $V_{fl} = 0.3$, 30% reduction this results in darker grey values for those which are already relatively low, and brighter grey values for those that are

relatively high with the intensity now more closely matched to the reference volume $V_{fl} = 0.3$, 50% reduction. The application of the match contrast function was similarly applied to the target volume of the as- cast condition against the reference volume $V_{fl} = 0.3$, 50% reduction. With the grey values now comparable, the same segmentation process can be applied across all volumes; a marker based watershed algorithm. This segmentation method is analogous to the flood filling of a topographical map where the height is equivalent to the grey value intensity. From initial markers of the individual phases the algorithm allows a gradient dependent flood filling of the map; where the gradient magnitude of grey value in the flooding direction is relatively high the filling is slower, and conversely where this gradient is relatively low the filling is faster. The volumes contained three distinct phases; pore, matrix and particles that were assigned initial threshold markers of 0-15000, 20000-25000 and > 30000 grey values respectively. From these basins the watershed algorithm filled the rest of the volume for each of the phases simultaneously, resulting in the segmentation to be analysed.

Figure 5 shows the fully segmented volume of Al-Cu-TiB$_2$ in-situ composites. Aluminium matrix is represented in green, TiB$_2$ particles in red and pores in blue color in figure 5. It is worth mentioning here that for better visualisation, we have isolated the pores from the matrix phase and particles in the top portion of sample volume and similarly TiB$_2$ particles were isolated from other two phases in the middle region of the sample volume as represented by their respective colors in figure 5. The 3D reconstructed XCT image shows the packing of the aluminium matrix along with the TiB$_2$ particles and included pores in the composite.

Figure 6 shows the porosity distribution in Al-4.5Cu-5TiB$_2$ composites for the entire volume. For better visualisation of porosity, we have removed matrix phase and particles from the entire volume. The as-cast Al-4.5Cu-5TiB$_2$ composite shows that the porosity varies greatly in size distribution, whereas the composite deformed up to 30% exhibits minimal porosity as compared to other two

7

conditions. Further, the composite subjected to 50% deformation show a higher amount of porosity compared to the 30% deformation. Similar observations of increase in porosity with increase in compressive deformation in semi-solid state in Al-Cu alloy was made by Kareh et al[37] in their in-situ synchrotron XCT measurements. They found that semi-solid alloy with a solid fraction greater than 70% causes porosity formation and subsequently leads to cracking of the sample. Phillion et al [38, 39] and Cao et al [40] studied the semi-solid alloy behaviour under compressive loading conditions. They found that initial stage of compression led to an increase in porosity and with further compression resulting shear induced dilation which drops the local pressure and causes small internal pores to coalesce and grow.

In our study, the 30% reduction has drastically reduced the frequency of pores and the average pore size is found to be relatively smaller, but with increasing forging reduction to 50%, porosity was found to be slightly increased as visualised in figure 7(c). It is evident from figure 7(c) that small pores coalesce together to form bigger size pores in the 50% deformed composite. Further investigations such as in-situ XCT study in semi-solid Al-TiB$_2$ composites are essential to understand the mechanism of porosity formation under compressive loading conditions. As shown in figure 7(a), the single largest pore size in the as-cast composite was found to be 30 μm wide and 40 μm in length. This was significantly smaller in the 30% deformed sample and 50% deformed sample, 3 μm wide and 2 μm length 10μm width and 9 μm length respectively as shown in figure 7(b) and 7(c). Also, the pores in as-cast composite are observed to be densely interconnected which is not observed in the 30% forge reduction.

Figure 8 shows a thin slice of the segmented TiB$_2$ particles in Al-Cu-TiB$_2$ composites. As shown in figure 8, the as-cast sample exhibits relatively large size clusters of TiB$_2$ particles that are densely interconnected, while forged samples have distribution of small sized TiB$_2$ particles in the matrix as shown in Figure 8(b) and 8(c) respectively. Figure 9 shows the individual single largest

8

particle/cluster obtained from XCT data for Al-Cu-TiB$_2$ composite. The single largest TiB$_2$ cluster size in as-cast Al-4.5Cu-5TiB$_2$ composite (Figure 9(a)) is approximately 200 µm wide and 400 µm in length. Whereas the largest TiB$_2$ cluster size in 30% deformed sample is 30 µm wide and 60 µm length (Figure 9(b)) and the 50% deformed sample, with a 40 µm width and 120 µm length as show in figure 9(c).

XCT data was analysed in order to quantify the porosity and TiB$_2$ particle distribution in the composite. Figure 10(a) represents the quantified size distribution of porosity in Al-Cu-TiB$_2$ in-situ composites. Though porosity is present in the forged samples, it is much small in average size compared to as-cast pores. Further, the average size of pores in 30 % reduction sample is smaller compared to 50% reduction sample. As shown in Figure 10(b) the higher number of small size particles were present in 30% reduction sample than the 50% reduction samples.

To further interrogate the distribution of particulates, a local thickness analysis was conducted on the segmented matrix phase in ImageJ (open source) using the plugin by Bob Dougherty (Optinav, USA). The algorithm calculates the local thickness using the method described by Hildebrand and Ruesgsegger [43], where each voxel is assigned a value equal to the diameter of the largest sphere that fits inside the object and contains the point. Example slices of the thickness calculation for the matrix are shown in Figure 11, where pores and particles have been masked out so appear as a zero thickness.

Qualitative observation between the two 0.3 V$_f$ conditions at 30% and 50% reduction demonstrate regions of greater local thickness in the 50% reduction than the 30% reduction. This is consistent with the greater amount of agglomeration of particles observed in the 50% reduction. Further, the distribution of thickness is relatively uniform in the 30% reduction in comparison to the 50% reduction that shows a large number of localised regions with a greater than average local thickness. Comparing this to the as-cast condition, the non-uniformity of clustered particles and pores is obvious, resulting in a number of regions with both relatively high and low local thicknesses. The

mean local thickness was 9.14 microns, 9.23 microns and 9.74 microns for the 30% reduction, 50% reduction and as-cast conditions respectively. The larger mean in the as-cast condition is a result of the non-uniformity of agglomerate distribution that has led to expanses with no particulate. The slightly lower mean in the 30% reduction than the 50% reduction is a result of the finer packing found in the 30% reduction.

The present study using XCT technique clearly shows that the application of forging in semi-solid state drastically reduces the porosity and helps in deagglomeration of TiB$_2$ particle clusters and uniform distribution of particles in the matrix. 3D visualisation and quantified information of porosity and TiB$_2$ particle distribution obtained from XCT results are helpful not only in optimising the casting and semi-solid processing of composites, but also useful in modelling the mechanical and performance properties of the composites. [9,40,41,42].

4. Summary

- In-situ Al-4.5%Cu-5%TiB$_2$ metal matrix composites were prepared using salt-reactions by casting methods. The cast composites were semi-solid forged at 0.3 V$_{fl}$ using two forging reduction such as 30% reduction and 50% reduction.

- Submicron resolution XCT technique was used to study porosity distribution and TiB$_2$ particle distribution in as-cast as well as in semi-solid forged MMCs.

- XCT results showed that the size of forging in semi solid state significantly decreases the porosity as compared to as-cast condition. However, the porosity was found to be slightly increased with increasing forge reduction from 30% to 50% reduction.

- Clusters of TiB$_2$ particles were found be bigger in average size in as-cast composites compared to semi-solid forged composites. It was observed that 30% reduction resulted in uniform distribution of particles in the matrix and also helped in reducing the clustering of particles in the matrix as compared to as-cast and 50% reduction samples.

10

- XCT as well as optical and SEM microscopy results show that the application of forging in semisolid state helps reducing the porosity and uniform distribution of TiB_2 particles in-situ Al-TiB_2 composites. These results will be very useful in modelling the mechanical and performance properties of Al-Cu-TiB_2 metal matrix composites.

Acknowledgments

5. References

[1]   T.M. Pollock, Weight Loss with Magnesium Alloys, Science (80-.). 328 (2010) 986–987.
[2]   D.J. Lloyd, Particle reinforced aluminium and magnesium matrix composites, Int. Mater. Rev. 39 (1994) 1–23.
[3]   I.A. Ibrahim, F.A. Mohamed, E.J. Lavernia, Particulate reinforced metal matrix composites ? a review, J. Mater. Sci. 26 (1991) 1137–1156. doi:10.1007/BF00544448.
[4]   R.H. Jones, Metal Matrix Composites, Environ. Eff. Eng. Mater. (2001) 375–390. doi:10.1007/978-94-011-1266-6.
[5]   B.S. Murty, S. a. Kori, M. Chakraborty, Grain refinement of aluminium and its alloys by heterogeneous nucleation and alloying, Int. Mater. Rev. 47 (2002) 3–29. doi:10.1179/095066001225001049.
[6]   S. Tjong, Microstructural and mechanical characteristics of in situ metal matrix composites, Mater. Sci. Eng. R Reports. 29 (2000) 49–113. doi:10.1016/S0927-796X(00)00024-3.
[7]   B. Das, S. Roy, R.N. Rai, S.C. Saha, Engineering Science and Technology , an International Journal Development of an in-situ synthesized multi-component reinforced Al – 4 . 5 % Cu – TiC metal matrix composite by FAS technique – Optimization of process parameters, 19 (2016) 279–291.
[8]   M. Emamy, M. Mahta, J. Rasizadeh, Formation of TiB2 particles during dissolution of TiAl3 in Al–TiB2 metal matrix composite using an in situ technique, Compos. Sci. Technol. 66 (2006) 1063–1066. doi:10.1016/j.compscitech.2005.04.016.
[9]   M. Karbalaei Akbari, H.R. Baharvandi, K. Shirvanimoghaddam, Tensile and fracture behavior of nano/micro TiB2 particle reinforced casting A356 aluminum alloy composites, Mater. Des. 66 (2015) 150–161. doi:10.1016/j.matdes.2014.10.048.
[10]   D. Chen, M.L. Wang, Y.J. Zhang, X.F. Li, Z. Chen, N.H. Ma, et al., Microstructure and mechanical properties of TiB 2 /2219 composites, Mater. Res. Innov. 18 (2014) S4–514–S4–518. doi:10.1179/1432891714Z.000000000731.
[11]   R.W. Hamilton, M.F. Forster, R.J. Dashwood, P.D. Lee, Application of X-ray tomography to quantify the distribution of TiB2 particulate in aluminium, Scr. Mater. 46 (2002) 25–29. doi:10.1016/S1359-6462(01)01190-3.
[12]   F. Chen, F. Mao, Z. Chen, J. Han, G. Yan, T. Wang, et al., Application of synchrotron radiation X-ray computed tomography to investigate the agglomerating behavior of TiB2 particles in aluminum, J. Alloys Compd. 622 (2015) 831–836. doi:10.1016/j.jallcom.2014.10.190.

[13]   S. F. Corbin, D. S. Wilkinson, The influence of particle distribution on the mechanical response of a particulate metal matrix composite, Acta metall, mater. 42(1994), 1311-1318.

[14]   R. Mehrabian, R.G. Riek, M.C. Flemings, Preparation and Casting of Metal-Particulate Non-Metal Composites, 5 (1974) 1–7.

[15]   H. Atkinson, Modelling the semisolid processing of metallic alloys, Prog. Mater. Sci. 50 (2005) 341–412. doi:10.1016/j.pmatsci.2004.04.003.

[16]   Ł. Rogal, J. Dutkiewicz, H.V. Atkinson, L. Lityńska-Dobrzyńska, T. Czeppe, M. Modigell, Characterization of semi-solid processing of aluminium alloy 7075 with Sc and Zr additions, Mater. Sci. Eng. A. 580 (2013) 362–373. doi:10.1016/j.msea.2013.04.078.

[17]   I.G. Siddhalingeshwar, M.A. Herbert, M. Chakraborty, R. Mitra, Effect of mushy state rolling on age-hardening and tensile behavior of Al-4.5Cu alloy and in situ Al-4.5Cu-5TiB2 composite, Mater. Sci. Eng. A. 528 (2011) 1787–1798. doi:10.1016/j.msea.2010.11.027.

[18]   M.A. Herbert, C. Sarkar, R. Mitra, M. Chakraborty, Microstructural evolution, hardness, and alligatoring in the Mushy state rolled cast Al-4.5Cu alloy and In-situ Al4.5Cu-5TiB2 composite, Metall. Mater. Trans. A Phys. Metall. Mater. Sci. 38 A (2007) 2110–2126. doi:10.1007/s11661-007-9264-9.

[19]   A.M. Samuel, A. Gotmare, F.H. Samuel, Effect of solidification rate and metal feedability on porosity and SiC / Al_2O_3 particle distribution in an Al-Si-Mg (359) alloy, 3538 (1995) 301–315.

[20]   S.G. Lee, A. M. Gokhale, G.R. Patel, M. Evans, Effect of process parameters on porosity distributions in high-pressure die-cast AM50 Mg-alloy, Mater. Sci. Eng. A. 427 (2006) 99–111. doi:10.1016/j.msea.2006.04.082.

[21]   Y. Hangai, S. Kitahara, Quantitative evaluation of porosity in aluminum alloy die castings by fractal analysis of spatial distribution of area, Mater. Des. 30 (2009) 1169–1173. doi:10.1016/j.matdes.2008.06.025.

[22]   P.M. Mummery, B. Derby, P. Anderson, G.R. Davis, J.C. Elliott, X-ray microtomographic studies of metal matrix composites using laboratory X-ray sources, J. Microsc. 177 (1995) 399–406. doi:10.1111/j.1365-2818.1995.tb03570.x.

[23]   J.J. Williams, N.C. Chapman, V. Jakkali, V.A. Tanna, N. Chawla, X. Xiao, et al., Characterization of Damage Evolution in SiC Particle Reinforced Al Alloy Matrix Composites by In-Situ X-Ray Synchrotron Tomography, Metall. Mater. Trans. A. 42 (2011) 2999–3005. doi:10.1007/s11661-011-0718-8.

[24]   J.J. Williams, Z. Flom, A.A. Amell, N. Chawla, X. Xiao, F. De Carlo, Damage evolution in SiC particle reinforced Al alloy matrix composites by X-ray synchrotron tomography, Acta Mater. 58 (2010) 6194–6205. doi:10.1016/j.actamat.2010.07.039.

[25]   S. Terzi, R. Daudin, J. Villanova, P. Srirangam, P. Lhuissier, X-Ray tomography and Small-angle neutron scattering characterization of nano-composites : static and in situ experiments, in: TMS 2014, n.d.

[26]   I.G. Watson, M.F. Forster, P.D. Lee, R.J. Dashwood, R.W. Hamilton, a. Chirazi, Investigation of the clustering behaviour of titanium diboride particles in aluminium, Compos. Part A Appl. Sci. Manuf. 36 (2005) 1177–1187. doi:10.1016/j.compositesa.2005.02.003.

[27]   F. de Andrade Silva, J.J. Williams, B.R. Müller, M.P. Hentschel, P.D. Portella, N. Chawla, Three-Dimensional Microstructure Visualization of Porosity and Fe-Rich Inclusions in SiC Particle-Reinforced Al Alloy Matrix Composites by X-Ray Synchrotron Tomography, Metall. Mater. Trans. A. 41 (2010) 2121–2128. doi:10.1007/s11661-010-0260-0.

[28]   N.C. Chapman, J. Silva, J.J. Williams, N. Chawla, X. Xiao, Characterisation of thermal cycling induced cavitation in particle reinforced metal matrix composites by three-dimensional (3D) X-ray synchrotron tomography, Mater. Sci. Technol. 31 (2015) 573–578. doi:10.1179/1743284714Y.0000000582.

[29]   E. Maire, P.J. Withers, Quantitative X-ray tomography, Int. Mater. Rev. 59 (2014) 1–43. doi:10.1179/1743280413Y.0000000023.

[30]   J.Y. Buffière, E. Maire, P. Cloetens, G. Lormand, R. Fougères, Characterization of internal damage in a MMC$_p$ using X-ray synchrotron phase contrast microtomography, Acta Mater. 47 (1999) 1613–1625. doi:10.1016/s1359-6454(99)00024-5.

[31]   L. Babout, Y. Brechet, E. Maire, R. Fougères, On the competition between particle fracture and particle decohesion in metal matrix composites, Acta Mater. 52 (2004) 4517–4525. doi:10.1016/j.actamat.2004.06.009.

[32]   A. Ferre, S. Dancette, E. Maire, Damage characterisation in aluminium matrix composites reinforced with amorphous metal inclusions, Mater. Sci. Technol. 31 (2014) doi:10.1179/1743284714Y.0000000619.

[33]   N. Limodin, L. Salvo, E. Boller, M. Suery, M. Felberbaum, S. Gailliegue, K. Madi, In situ and real-time 3-D microtomography investigation of dendritic solidification in an Al-10 wt.% Cu alloy, Acta Mater. 57 (2009) 2300–2310. doi:10.1016/j.actamat.2009.01.035.

[34]   M. De Giovanni, J.M. Warnett, M. A. Williams, N. Haribabu, P. Srirangam, X-ray tomography investigation of intensive sheared Al–SiC metal matrix composites, Mater. Charact. 110 (2015) 258–263. doi:10.1016/j.matchar.2015.11.003.

[35]   M. Sikandar, H. Khiyal, A. Khan, A. Bibi, Modified Watershed Algorithm for Segmentation of 2D Images, 6 (2009).

[36]   H. Digabel, C. Lantuéjoul, Iterative algorithims, in: Actes Du Second Symp. Eur. d'Analyse Quant. Des Microstruct. En Sci. Des Matériaux., 1977: pp. 85–99.

[37]   K.M. Kareh, P.D. Lee, R.C. Atwood, T. Connolley, C.M. Gourlay, Revealing the micromechanisms behind semi-solid metal deformation with time-resolved X-ray tomography., Nat. Commun. 5 (2014) 4464. doi:10.1038/ncomms5464.

[38]   A. B. Phillion, S.L. Cockcroft, P.D. Lee, A new methodology for measurement of semi-solid constitutive behavior and its application to examination of as-cast porosity and hot tearing in aluminum alloys, Mater. Sci. Eng. A. 491 (2008) 237–247. doi:10.1016/j.msea.2008.01.078.

[39]   A. B. Phillion, S.L. Cockcroft, P.D. Lee, X-ray micro-tomographic observations of hot tear damage in an Al–Mg commercial alloy, Scr. Mater. 55 (2006) 489–492. doi:10.1016/j.scriptamat.2006.03.035.

[40]   B. Cai, S. Karagadde, L. Yuan, T.J. Marrow, T. Connolley, P.D. Lee, In situ synchrotron tomographic quantification of granular and intragranular deformation during semi-solid compression of an equiaxed dendritic Al–Cu alloy, Acta Mater. 76 (2014) 371–380. doi:10.1016/j.actamat.2014.05.035

[41]   V. Favier, H.V. Atkinson, Micromechanical modelling of the elastic–viscoplastic response of metallic alloys under rapid compression in the semi-solid state, Acta Mater. 59 (2011) 1271–1280. doi:10.1016/j.actamat.2010.10.059.

[42]   R. Rahmani Fard, F. Akhlaghi, Effect of extrusion temperature on the microstructure and porosity of A356-SiCp composites, J. Mater. Process. Technol. 187-188 (2007) 433–436. doi:10.1016/j.jmatprotec.2006.11.077.

[43] T. Hildebrand and P. Ruesgsegger, A new method for the model-independent assessment of thickness in three-dimensional images, J. of Microscopy 185 (1996) 67-75.
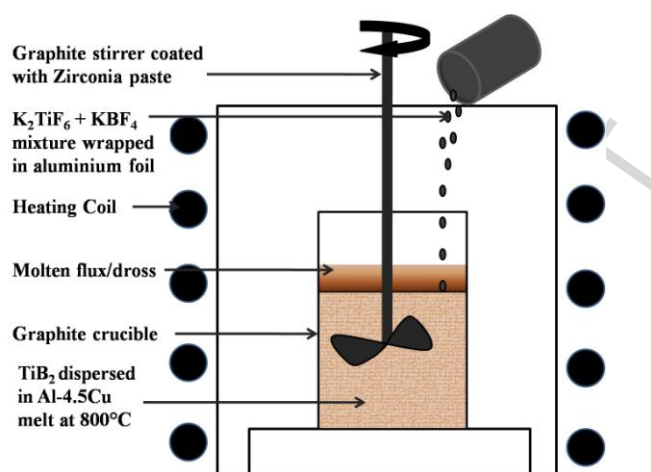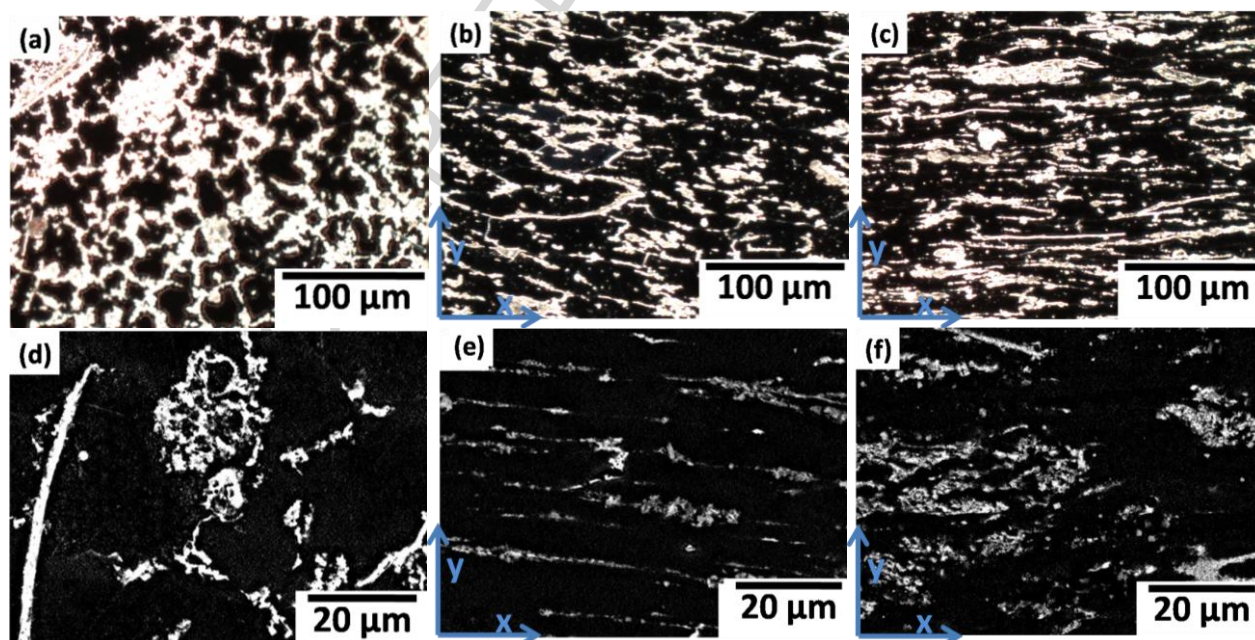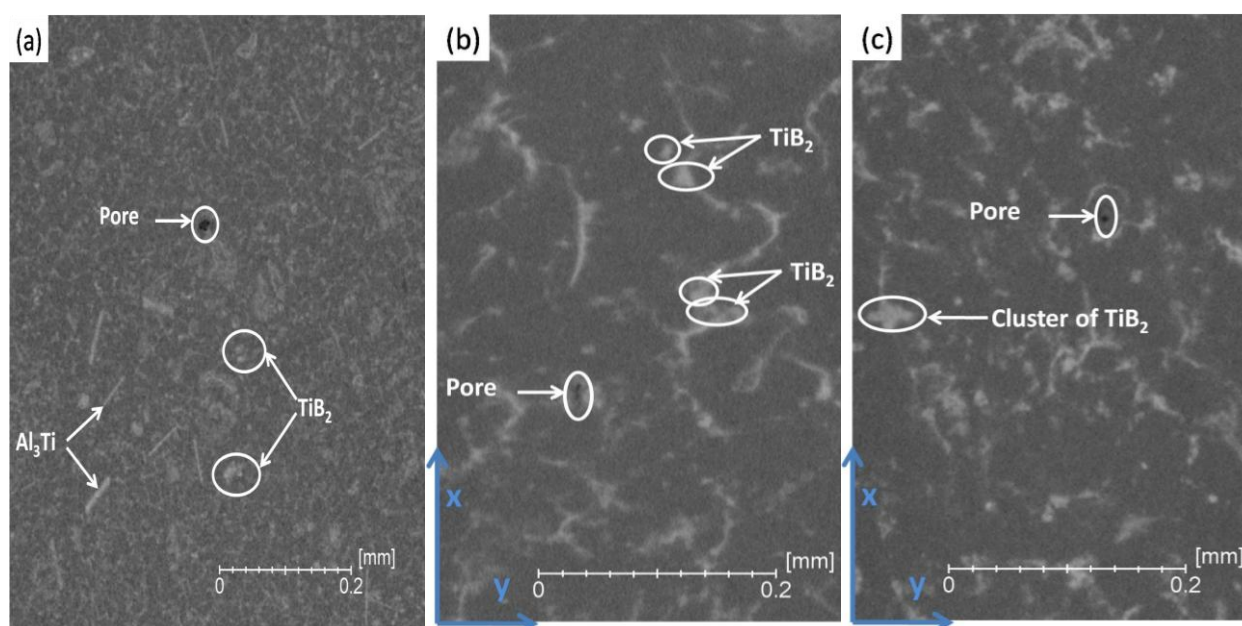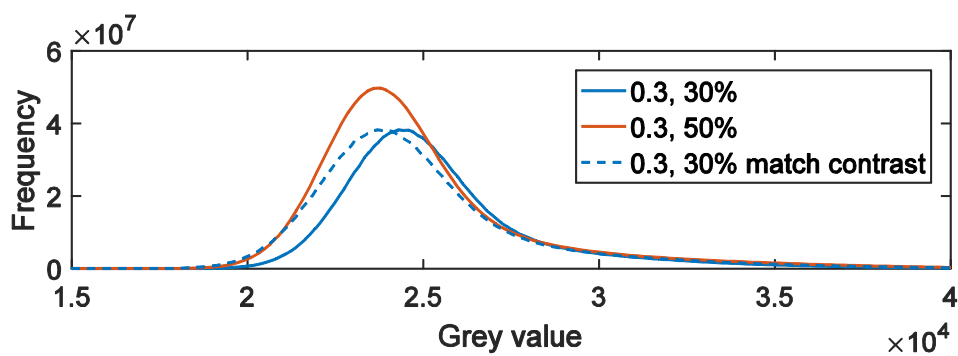
Graphite stirrer coated with Zirconia paste

$K_2TiF_6 + KBF_4$ mixture wrapped in aluminium foil

Heating Coil

Molten flux/dross

Graphite crucible

TiB_2 dispersed in Al-4.5Cu melt at 800°C

Fig. 1.

Fig. 2.

Fig. 3

15

(a)

(b)

Fig. 4.

16

(a)

(b)

(c)

0.2 mm

0.1 mm

0.1 mm

Fig. 5.

Fig. 6.

Fig.7.

(a)

50 µm

(b)

70 µm

(c)

70 µm

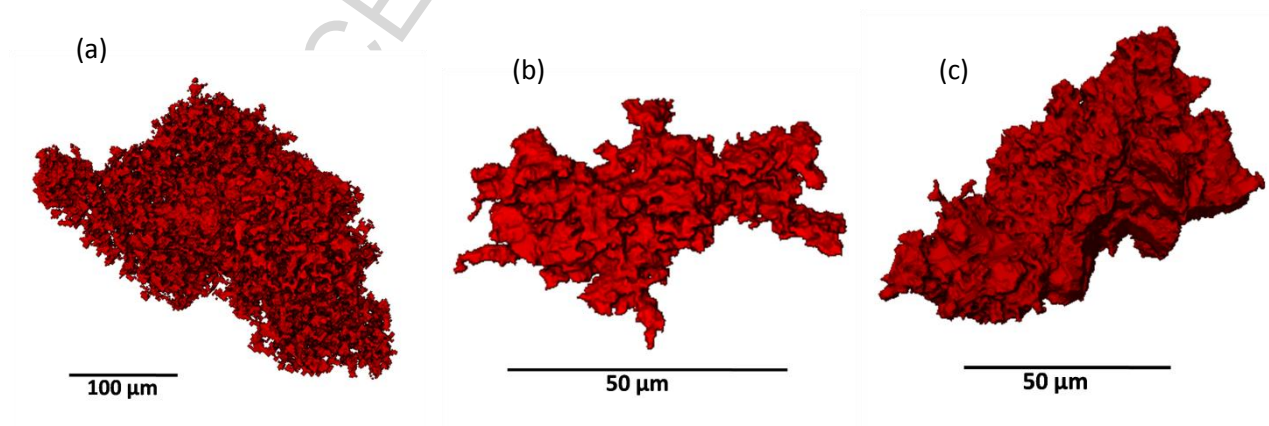**Fig. 8.**

(a)

100 µm

(b)

50 µm

(c)

50 µm
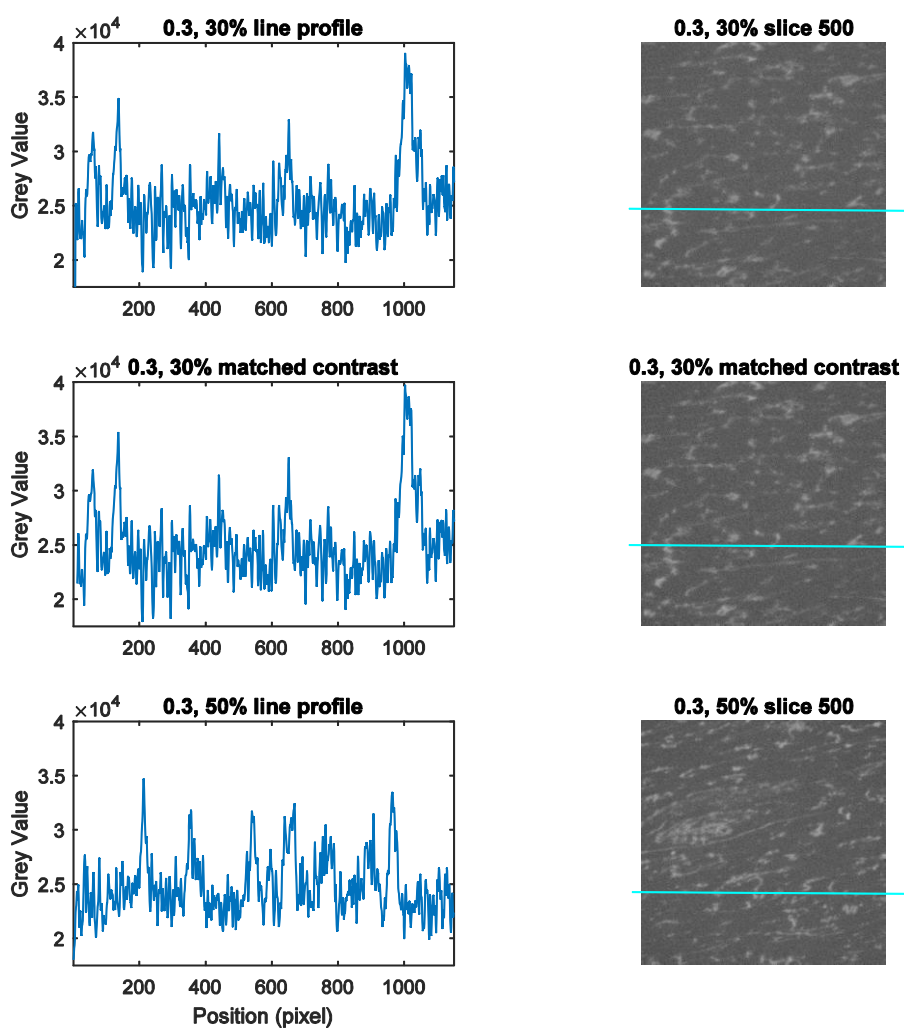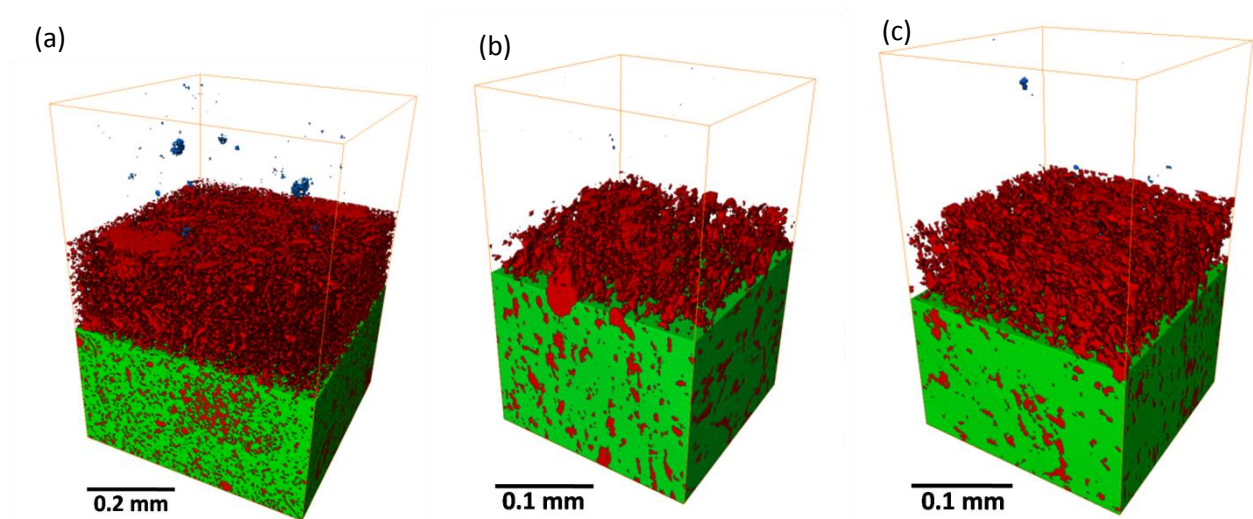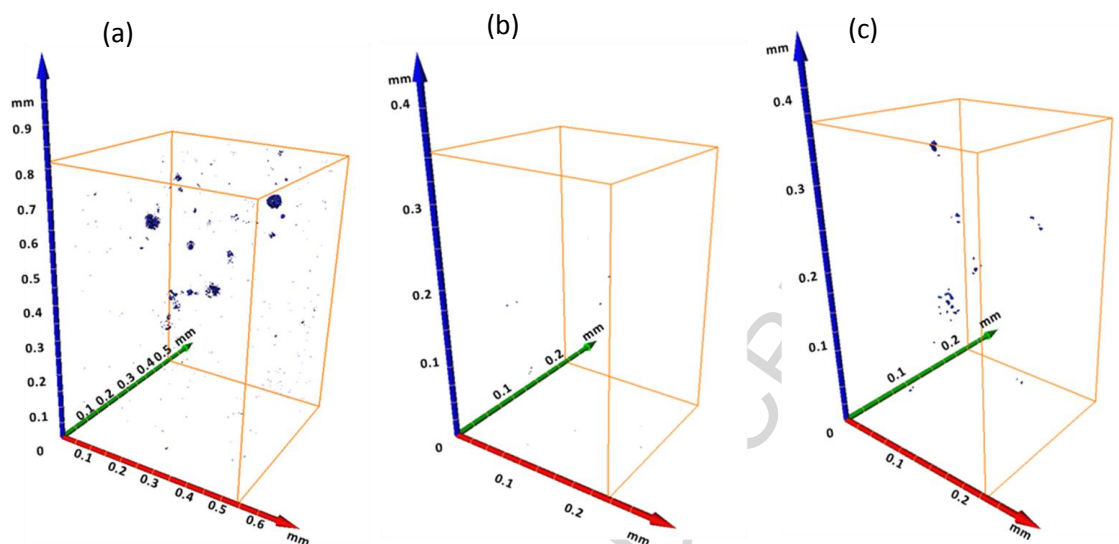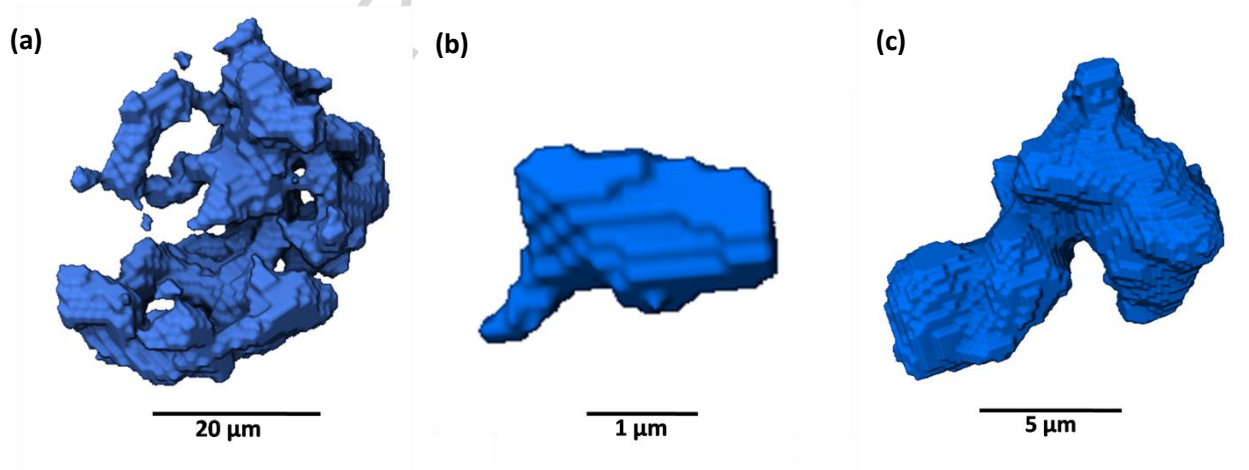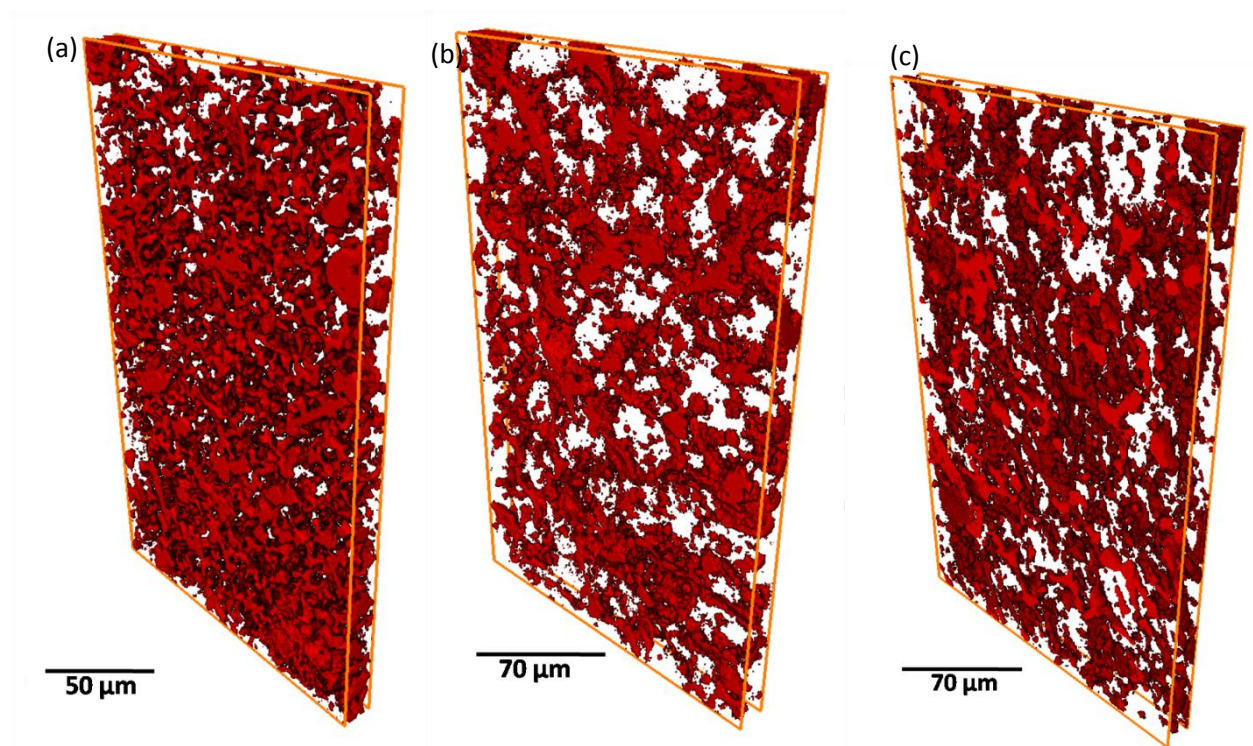
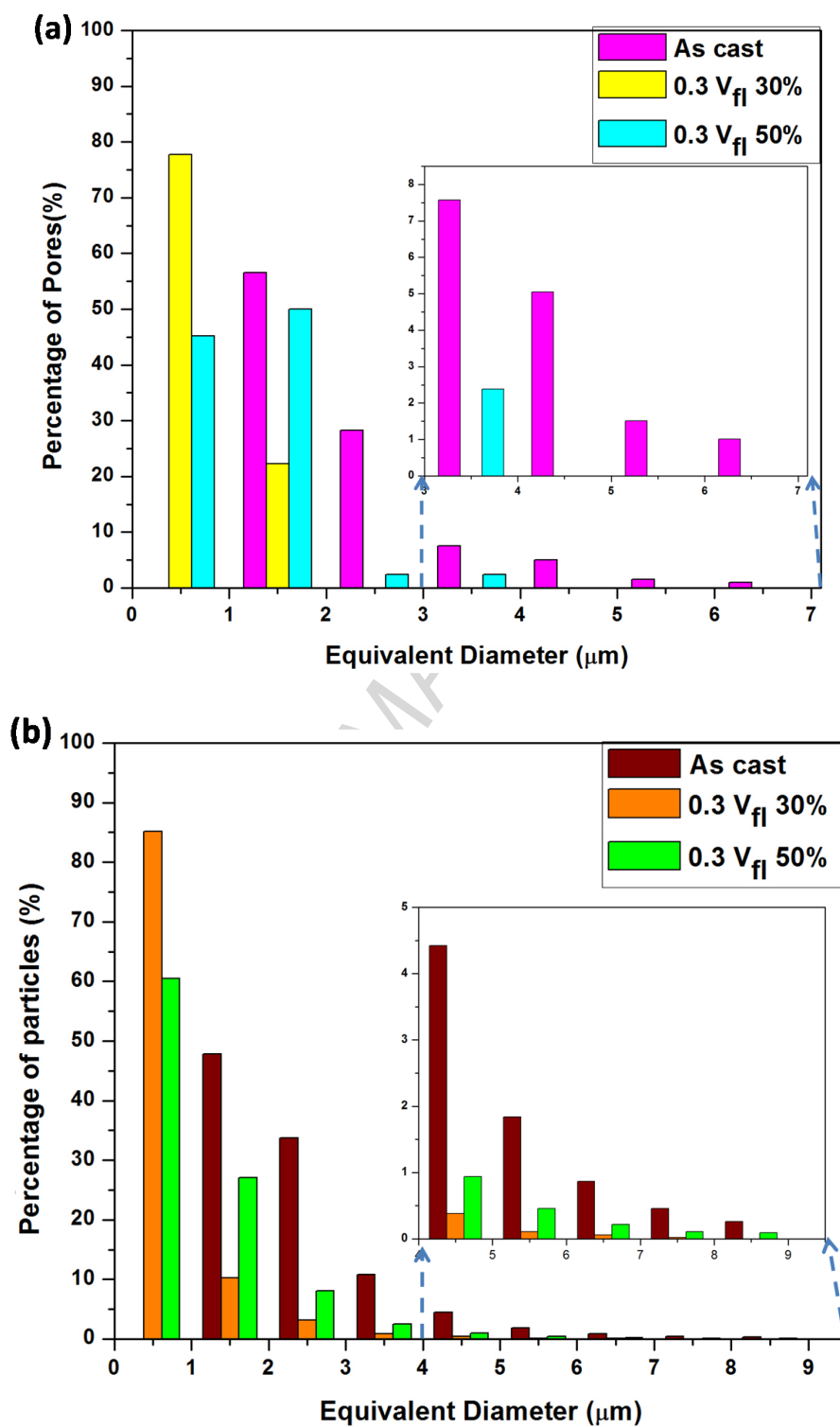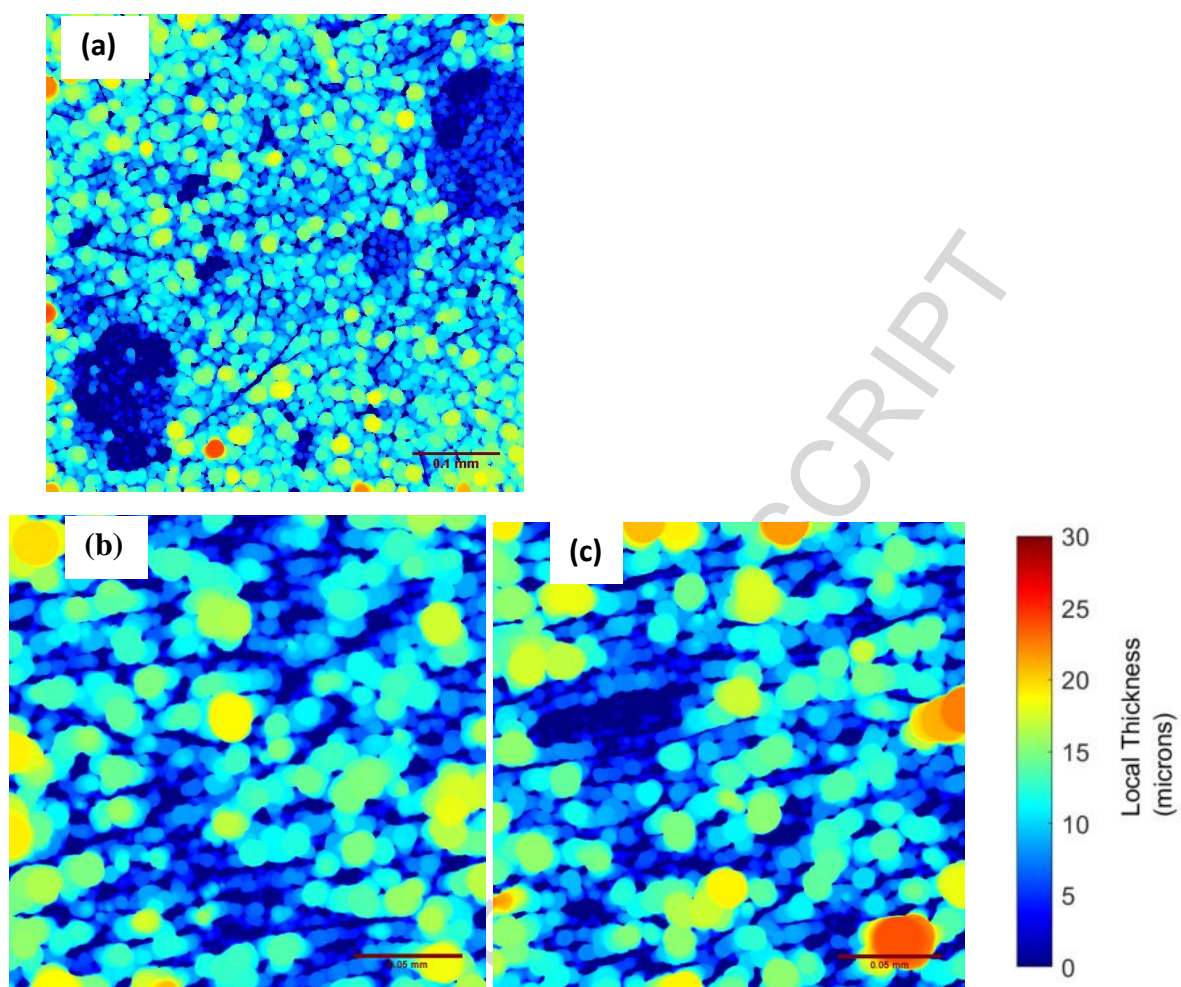**Fig. 9.**

Fig. 10

Fig.11

21

Figure captions

Fig. 1. Schematic of flux assisted synthesis of in-situ Al-Cu-TiB$_2$ composites.

Fig. 2. Optical and SEM microstructure of Al-4.5Cu-5TiB$_2$ composite (a) and (d) as-cast condition (b) and (e) 0.3V$_{fl}$, 30% reduction (c) and (f) 0.3V$_{fl}$, 50% reduction. ('y' represents the forging direction).

Fig. 3. Orthogonal slices of Al-4.5Cu-5TiB$_2$ composite (a) as-cast condition (b)V$_{fl}$=0.3, 30% reduction (c) V$_{fl}$ = 0.3, 50% reduction. ('y' represents the forging direction).

Fig. 4. a) Grey level histograms showing: V$_{fl}$ = 0.3, 30% reduction; V$_{fl}$ = 0.3, 50% reduction; and the match contrast function applied to V$_{fl}$ = 0.3, 30% reduction with the reference volume V$_{fl}$ = 0.3, 50% reduction. b) Line profiles of each volume showing how the match contrast function has affected the grey values in the case of V$_{fl}$ = 0.3, 30% reduction, resulting in greater agreement of grey values for each phase.

Fig. 5. 3-D reconstructed XCT images showing porosity (blue colour) as well as particles (red colour) in Al matrix (green colour) in-situ composite (a) as-cast condition (b) 0.3 V$_{fl}$, 30% reduction (c) 0.3 V$_{fl}$, 50% reduction.

Fig. 6. 3-D XCT showing porosity distribution in Al-4.5Cu-5TiB$_2$ composite (a) as-cast condition (b) 0.3 V$_{fl}$, 30% reduction (c) 0.3V$_{fl}$, 50% reduction.

Fig.7. XCT rendering of single largest individual pore in Al-4.5Cu-5TiB$_2$ composite (a) as -cast condition (b) 0.3 V$_{fl}$, 30% reduction (c) 0.3 V$_{fl}$, 50% reduction.

Fig. 8. 3-D XCT showing particle clusters (after removing porosity and Al matrix) in Al-4.5Cu-5TiB$_2$ composite (a) as-cast condition (b) 0.3 V$_{fl}$, 30% reduction (c) 0.3 V$_{fl}$, 50% reduction.

Fig. 9. XCT rendering of single largest individual particle/cluster in Al-4.5Cu-5TiB$_2$ composite (a) as-cast condition (b) = 0.3 V$_{fl}$, 30% reduction (c) = 0.3 V$_{fl}$, 50% reduction.

Fig.10. Quantified size distribution of (a) porosity (b) TiB$_2$ particles/clusters.

Fig.11. 2D slices of the local thickness calculation performed in Image J (a) as-cast condition, (b) 30% reduction, (c) 50% reduction.

Table Caption

Table 1: X-ray tomography scanning parameters.

X-ray tomography studies on porosity and particle size distribution in cast in-situ Al-Cu-TiB$_2$ semi-solid forged composites

Highlights:

- XCT was used to visualise 3D internal structure of Al-Cu-TiB$_2$ MMCs.
- Al-Cu-TiB$_2$ MMC was prepared by casting using flux assisted synthesis method.
- TiB$_2$ particles and porosity size distribution were evaluated.
- Results show that forging in semi-solid condition decreases the porosity content and improve the particle dispersion in MMCs.